Cold Regions Science and Technology 193 (2022) 103425

Contents lists available at ScienceDirect

Cold Regions Science and Technology

journal homepage: www.elsevier.com/locate/coldregions

# Ice load measurements on Rätan concrete dam using different sensor types

Rikard Hellgren [a,*], Chris Petrich [b], Bård Arntsen [b], Richard Malm [a]

[a] Division of Concrete Structures, Department of Civil and Architectural Engineering, KTH Royal University of Technology, Sweden
[b] SINTEF Narvik, Norway

ARTICLE INFO

*Keywords:*
Ice load
Concrete dam
Load panel
Stress cells
Ice pressure
ice thickness

ABSTRACT

Concrete dams in cold regions are designed to withstand loads from the ice sheet on top of the reservoir. However, the ice load's magnitude and return period are among the most considerable uncertainties in safety assessments of concrete dams. In a previous study, the development and installation of a $1 \times 3$ m$^2$ prototype ice load panel attached at the upstream face of a concrete dam was presented. The panel is large enough for the ice sheet's cross-section to remain in contact with the panel as the water level varies, and it measures the total ice load without interpolation. This paper presents measurement results from the load panel from winters 2018–19 and 2019–20, an update to the measurement design, and additional ice pressure measurements with traditional stress cells. The panel measured seasonal maximum ice loads of 100 and 200 kN/m for the two winters, respectively. Winter 2019–20, when the panel measured the largest loads, was mild for the location, with great ice thickness near the dam face (1.2 m) and an almost snow-free ice sheet throughout the winter. Two $2.75 \times 1.75$ m$^2$ dummy panels were installed adjacent to the load panel prior to the winter 2019–20 to minimize the load panel's protruding effect. These panels significantly reduced the local impact, as evident by the crack-pattern of the ice sheet near the load panel. The load panel recorded large ice loads (>75 kN/m) for all combinations with increasing/decreasing air temperature and/or water level. Identification of temperature change events and water level change events during the winters, shows that a change in air temperature, water level, or any combination of these, is not sufficient alone to explain large ice loads at Rätan dam. These findings suggest that other conditions must be satisfied before a water level or temperature change results in large ice loads. In February 2020, three panels consisting of a steel frame with four stress cells on each were placed on the dummy panels' upstream face, and one single stress cell was placed 6 m out in the reservoir in front of the load panel. The majority of the stress cells recorded ice pressure larger than their measurement range. At the end of the ice season, only two of the panels' twelve stress cells were still functional, and the ice vastly deformed the steel frames. From the period before the frames were damaged and unrelated to the choice of interpolation method, the recordings by the three stress cell panels at the dam are among the historically largest inferred ice loads on dams.

## 1. Introduction

Concrete dams in cold regions are designed to withstand loads from the ice sheet on top of the reservoir. Those ice loads are often categorized as either static or dynamic. Static ice loads on a dam occur when the structure restrains a movement or expansion of the ice sheet, while dynamic ice loads are caused by the impact from a drifting ice flow. The static ice load at a dam is believed to be caused by three main mechanisms: restrained thermal expansion, change in the water level, and shear forces from the water and air flow under and above the ice (Carter et al., 1998; Comfort et al., 2003). The current design ice loads make up a significant fraction of the total horizontal forces considered in design, especially for smaller concrete dams. However, the ice loads' magnitude and return periods are among the most considerable uncertainties in dam safety assessments. The ice's properties make it difficult to model and theoretically determine the static ice load magnitude. Simultaneously, the quantity of measurements is inadequate to determine the ice load's magnitude from empirical data accurately.

Four categories of methods and procedures exist for measurement and empirical estimation of ice-structure interaction for fixed structures (Bjerkås, 2007): internal ice stress measurements; interfacial methods; structural response monitoring and hindcast calculations; and Newton's

* Corresponding author.
*E-mail address:* rikard.hellgren@byv.kth.se (R. Hellgren).

https://doi.org/10.1016/j.coldregions.2021.103425
Received 15 April 2021; Received in revised form 11 July 2021; Accepted 8 October 2021
Available online 13 October 2021

second law.

The first method, internal stress measurements with sensors that measure the stress in the ice sheet is the most common method used to measure ice loads on dams. Internal stress measurements are performed either by strain gauges or rectangular stress cells, also called flat-jacks (Cox and Johnson, 1983). Stress cells consist of an oil-filled sheet-pad with two rectangular plates, where the oil pressure between the sheets is measured continuously. The oil pressure after the pad is embedded in the ice sheet is assumed to correspond to the ice pressure perpendicular to the stress-cells' surface, neglecting eventual shear forces. These stress-cells are placed either in the reservoir or at the dam's face. As this is a local method, measurements at several depths are required to estimate the resultant force over the cross-section of the ice sheet (Comfort et al., 2003; Petrich et al., 2015).

The second method, the interfacial method generally consists of a load panel attached to the structure. The load panel usually consists of two rigid steel plates placed on each side of a material with a known stiffness. The ice pressure applied at the load panel is determined from the displacement of the material. For measurements of ice pressure on concrete dams, the interfacial method has mainly been applied using Carter panels. The Carter panel consists of four stress cell sensors, mounted on a 0.4 m wide, 1 m high, and 10 mm thick stainless steel plate to form a load panel (Carter et al., 1998; Morse et al., 2011).

The third method, structural response monitoring and hindcast calculations are two procedures where the ice load magnitude is estimated from the structure's response. In the first method, the structural behavior is monitored, and a change in that behavior is correlated to the magnitude of the ice load. In the second method, a hindcast calculation is performed after structural damage has been observed, and the required ice pressure to cause such damage is calculated. Even though monitoring of dam behavior is a relatively common dam safety measure, there are few reported cases where the ice load has been estimated from such measurements; exceptions are (Hellgren et al., 2017; Zhang et al., 2017, 2019). The fourth method is based on Newton's second law to determine the forces required to deaccelerate a drifting ice sheet. This method is more applicable for dynamic ice loads.

The development a prototype ice load panel and measurements of the ice load from 2016 to 2018 was presented by Hellgren et al. (2020). The panel was developed as a new interfacial method for dams, based on the ice load panels at Norströmsgrund lighthouse in the Gulf of Bothnia (Fransson, 2001; Schwarz and Jochmann, 2001). The $1 \times 3$ m$^2$ ice load panel is attached at the upstream face of the dam. Its size is large enough for the vertical cross-section of the ice sheet to remain in contact with the panel as the water level varies, and thus the total ice load is measured without interpolation. The panel can measure tensile forces and the position of the resultant force.

In the previous study, it was concluded that the panel disturbs the naturally formed ice sheet around the load panel. It could not be excluded that this disturbance affects the measurement results. This study addresses these issues by installing concrete slabs adjacent to the panel. These dummy panels create a longer undisturbed distance at the dam-ice interface near the load panel. Furthermore, additional ice load measurements where performed with three panels made of steel frame with four stress cells on each placed on the dummy panels' upstream face, and one stress cell in the reservoir. These additional measurements provide the opportunity to compare the two measurement methods and simultaneously study the variation in ice pressure along the dam line.

## 2. Methods and materials

This section provides a summary of the previous ice load measurements with the load panel. This includes a presentation of the dam where the measurements are performed, the development and installation of the panel, and some conclusions from previous measurements. The background is followed by a description of the fieldwork performed during winters 2018–19 and 2019–20, including ice and snow thickness measurement, an update of the measurement design, and measurements with stress cell panels. Thereafter, the section concludes with a presentation of the methods used for data analysis.

### 2.1. Summary of the previous project

The installation of the $1 \times 3$ m$^2$ sized load panel on the Rätan hydropower dam was performed in February 2016. The load panel consists of a steel plate and a lid made of homogeneous steel with a thickness of 160 mm. The lid is placed on three compression-only load cells and is attached to the steel plate by three pre-stressed screw connections in line with the load cells (LC). The pre-stressing of the screws enables both tensile and compressive forces from the ice to be measured. One load cell is placed in each corner of the top of the panel, and one is placed centric at the bottom; see Fig. 3 and Table 1 in the following section.

Rätan hydropower dam is a 31 m high traditional concrete buttress dam constructed in 1968 and located in the northern ice load region of Sweden. The dam was selected based on several criteria to ensure the measurement of significant ice loads; see Hellgren (2019) and Hellgren et al. (2020). The combination of a low reservoir amplitude, a long dam line, and a vertical front plate made the dam a suitable place to evaluate the ice load panel. The location of the dam's crest is at an altitude of +352.5 m above sea level (m.a.s.l), and the water level in the reservoir varies between the maximum water level (MAWL), +350.44 m.a.s.l, and the minimum operating level (MIWL), +349.94 m.a.s.l. This amplitude

**Table 1**
The position and zero reference values for all the load and stress cells. The position is the center of the respective sensor with origin at the maximum water level and the center of the load panel, *Y* increase upwards, and *X* increase to the right in the downstream direction. *kN for the load cells and kPa for the stress cells.

| Sensor | Short | *X* | *Y* | Winter | Zero recording | Last recording |
|---|---|---|---|---|---|---|
| | | m | m | years | kN/kPa* | |
| Load cell 1 | LC1 | 0.35 | 0.31 | 2018–19 | 86.8 | |
| | | | | 2019–20 | 93.6 | |
| Load cell 2 | LC2 | 0.35 | 0.31 | 2018–19 | 104.3 | |
| | | | | 2019–20 | 104.9 | |
| Load cell 3 | LC3 | 0.0 | −2.29 | 2018–19 | 112.1 | |
| | | | | 2019–20 | 117.0 | |
| Stress cell | CPA1 | 2.29 | 0.07 | 2019–20 | −2657 | 2020-03-14 |
| Stress cell | CPA2 | 2.29 | −0.12 | 2019–20 | −2800 | 2020-04-02 |
| Stress cell | CPA3 | 2.29 | −0.30 | 2019–20 | −2807 | 2020-05-10 |
| Stress cell | CPA4 | 2.29 | −0.47 | 2019–20 | −2724 | 2020-04-22 |
| Stress cell | CPB1 | 1.13 | 0.05 | 2019–20 | −2872 | 2020-03-30 |
| Stress cell | CPB2 | 1.13 | −0.26 | 2019–20 | −2550 | 2020-05-10 |
| Stress cell | CPB3 | 1.13 | −0.41 | 2019–20 | −2761 | 2020-03-30 |
| Stress cell | CPB4 | 1.13 | −0.65 | 2019–20 | −2535 | 2020-03-30 |
| Stress cell | CPC1 | −1.94 | −0.13 | 2019–20 | −2668 | 2020-03-18 |
| Stress cell | CPC2 | −1.94 | −0.34 | 2019–20 | −2637 | 2020-03-30 |
| Stress cell | CPC3 | −1.94 | −0.55 | 2019–20 | −2610 | 2020-03-30 |
| Stress cell | CPC4 | −1.94 | −0.76 | 2019–20 | −2621 | 2020-03-30 |
| Stress cell | CPD1 | 0.0 | −0.15[a] | 2019–20 | −2522 | 2020-04-02 |

[a] Reference to the top of the ice sheet.

is small enough so that the whole thickness of the ice can remain in contact with the panel.

The load panel is attached centric on monolith 15, with numbering from left to the right relative to the flow direction, see Fig. 1. The total dam length is approximately 600 m and the reservoir has a river-like shape with a length orthogonal to the dam of 4.3 km, which gives the length/width ratio 7.2. As an ice management strategy, de-icing by air circulator is used to remove the ice around the flood gates. The distance from the load panel to the nearest spillway gate is 31.5 m, which is believed to be sufficient so that the removed ice does not influence the ice load measured by the panel.

From the dam safety monitoring and the open database of the Swedish Meteorological and Hydrological Institute (SMHI, 2018), data are available for several external factors. In this study, the water level and air temperature measured at the dam was used in the analysis.

The load panel was installed on 24 February 2016 and has since then been left on the dam. Three winters of measurements were presented by Hellgren et al. (2020). Initially, the logger had to be started manually without remote access to check the status of the load panel. This lead to the loss of data from 22 February in the spring of 2018. Fig. 2 shows the timeline of all ice load measurements, including the start of logging, stop of logging, and periods with lost data. In a typical year, the ice sheet forms in early November and detaches from the dam wall in late April or early May.

The maximum recorded loads for these three winters were 160 kN/m, 160 kN/m, and 60 kN/m for the winters 2015–16, 2016–17, and 2017–18, respectively (Hellgren et al., 2020). A variation in water level, was according to Hellgren et al. (2020) the primary mechanism causing the peak ice loads. During periods when daily ice load peaks occurred, both the ice load and the water level followed a daily pattern related to the operation of the power station.

### 2.2. Improved measurement design

The main focus of this paper is the updates of the ice load measurements made during the winter 2019–20. This update include significant updates such as the installation of dummy panels, installation of additional ice load panels (stress cell panels) for comparative measurements, ice thickness and snow cover measurements, as well as some minor updates such as remote access to the computer and the replacement of the computer. The timeline of these updates are shown in Fig. 2.

#### 2.2.1. Ice and snow thickness

Starting from the winter 2018–19, the snow cover and the ice thickness in the reservoir near the load panel were measured. These measurements were taken by the operating staff of the dam owner at 0.3 m, 3 m, and 6 m distances perpendicular to the dam line. At each location, the operator drilled a hole in the ice and measured the ice thickness using a ruler with an edge hook. After that, the operator assessed the depth of the different types of ice, such as snow ice and black ice. During the winter 2018–19, the ice and snow thickness measurements were measured on five occasions (2018-12-19, 2019-01-22, 2019-02-20, 2019-03-28, and 2019-04-29. At the last measurement at the end of April, the ice sheet was no longer in contact with the load panel. The following winter, the ice thickness and snow cover were measured on five occasions (2020-01-09, 2020-02-12, 2020-02-27, 2020-03-13, 2020-03-27, and 2020-04-02).

In addition to the measurements, the ice thickness was estimated using Stefans equation where the ice thickness, $h_i$ is calculated from the accumulated freezing degree days (AFDD)

$$h_i = \alpha\sqrt{\mathrm{AFDD}}. \quad (1)$$

Here $\alpha$ is a coefficient to account for local conditions. In this study, $\alpha = 2.5$ was used.

#### 2.2.2. Dummy panels

One of the lessons learned from the previous winters was that the protruding load panel has a significant influence on the ice formation locally around the panel. To minimize this effect, dummy panels were installed adjacent to the load panel before the ice formation 2019. The purpose of the dummy panels is to create a longer undisturbed face at the ice load panel. These dummy panels were made with pre-cast concrete with dimensions $240 \times 1750 \times 2750\ \mathrm{mm}^3$. As the load panel

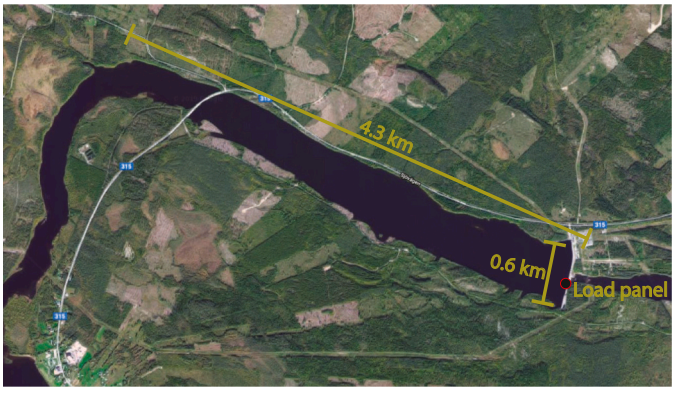


(a)

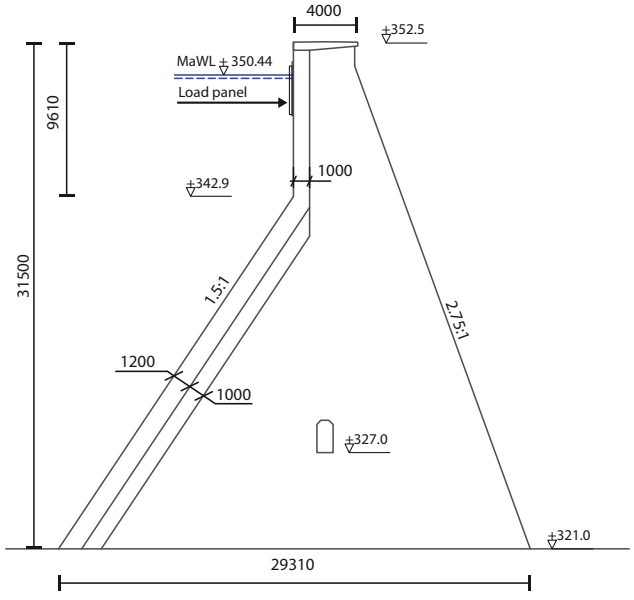


(b)

**Fig. 1.** Location and geometry of Rätan dam. (a) Shape of the reservoir, the load panel is placed at the marker, figure from Google (2019). (b) Side view of the buttress monolith where the panel is attached.

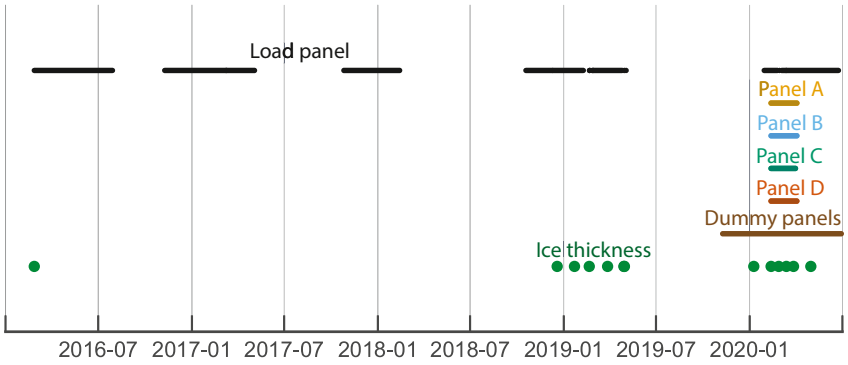


**Fig. 2.** Time line of the measurements and field work, the lines and dots show the time when a sensor was active or when a measurements was taken.

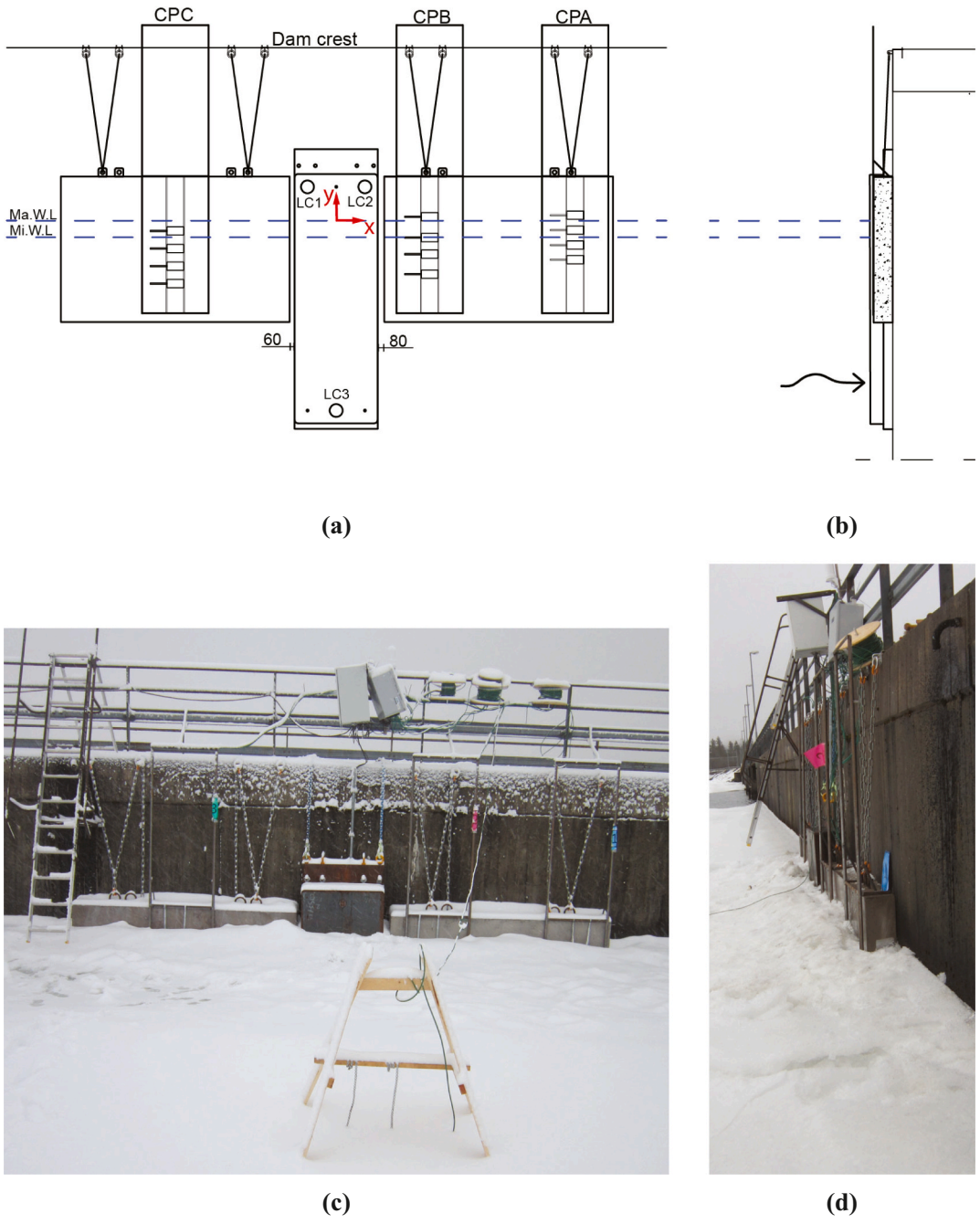


**Fig. 3.** Drawing and photographs of the measurement set up from 2020-01-11 (a) and (c) show the elevation and (b) and (d) the section.

protrudes 270 mm from the dam face, this design with a thickness of 240 mm ensures that the dummy panels do not unload the load panel. The dummy panels have a sufficient depth to cover the distance between the minimum and maximum water levels (0.5 m), including the expected ice thickness. The length of the dummy panels makes the total length of the even surface, including the load panel, to 6.5 m. The concrete had the following specifications; exposure class, XF3/XC4; w/c ratio, 0.50; strength class; C30/37; air pore ratio; 5%. Rebars with a diameter of 16 mm and center to center distance of 100 mm, were placed centric in the panels. On the upstream surface of the panels, timber formwork was used to mimic the surface of the dam.

The concrete panels were installed on 11 November 2019. At this time, the water was still open in most of the reservoir. However, the water near the dam was covered with an approximately two-centimeter thick sheet of snow-ice. This ice sheet was non-bearing and could easily be perforated with a wooden stick. Each panel was attached to the dam with four chains connected by shackles to two attachment points on the concrete. A sketch of the position of the concrete panels is shown in Fig. 3a and b, and photographs of the panels are shown in Fig. 3c and d. In their final position, the top of the dummy panels is at level +350.9. The gap between the concrete and the load panel is 60 mm and 80 mm for the left and right plate in the downstream-direction, respectively.

#### 2.2.3. New sensors

During the winter 2019–20, ice stress sensors were installed on the dummy panels. These sensors served two purposes; they facilitate the possibility to measure the variation in ice load along the dam, and they serves as a comparative measurement with the possibility to achieve convergence validation between the developed load panel and the stress cell panels. The idea is that if the load panel yields similar results as the stress cell panel, the belief in the correctness of both the load panel and the stress cell panels is increased. Before the winter 2019–20, a collaboration between KTH and SINTEF Narvik made it possible to use stress cells that were previously used for ice load measurements in Norway (Petrich et al., 2020). The cells were calibrated by the manufacturer to an accuracy of 0.5 kPa and has a range of measurement up to 1000 kPa. A total of thirteen stress cells were installed on the dam, distributed onto three frames with four sensors on each placed on the upstream face of the dummy panels and one sensor in the ice.

Each frame consists of two, 3-m long tubes with a diameter of 50 mm. At the top and bottom, between the tubes, two $12 \times 20$ mm$^2$ plates were attached so that the center to center distance between the tubes is 800 mm. In the middle of the frame, a shelf-like structure was attached, which was used to place the frames on the top of the concrete panels. Four stress cells were mounted on each of the three frames. The sensors were attached to two galvanized builders bands mounted between the horizontal steel plates. The cables for the sensors were pulled into the tube via a hole and out at the top to protect the cabling.

The panels were installed at the dam on 24 January 2020. Fig. 3 shows the location of the three panels. Panel C was placed in the middle of the left dummy panel, Panel B and Panel A were placed at the left and right edge of the right dummy panel, respectively. With this configuration, Panel B placed adjacent to the load panel, can be used to compare the measurement methods. Panel C has the longest undistributed ice contact, and the placement of Panel A allows the study of the distribution in ice load along the dam.

The ice closest to the dam was removed to install the stress cell panels. At the location of each panel, two holes with a diameter of 50 mm were drilled in the ice with a center-to-center distance of 1.0 m. An approximately 30 mm gap between the dam and ice was created by sawing the ice with a lightweight concrete saw and then mechanically removing ice attached to the dam wall with an ice spike. After the frames with the stress cell panels had been lowered in place, they were fixed to the top of the concrete panels with bolts. The thirteenth stress cell was placed directly in the ice sheet, centric on the load panel 6 m from the dam. An approximately 0.5 m long, 50 mm wide, and 0.2 m deep reef was created in the ice by combining drilling and sawing. The stress cell was placed in the bottom of the reef, with the vertical centre at 15 cm depth. It was attached to a sawhorse placed on the top of the ice sheet with to two builders' bands, see Fig. 3. The positions of all thirteen sensors are given in Table 1.

### 2.3. Line load calculation

The measured load by the load cells are calculated as,

$$\mathrm{LC}_i = \mathrm{LC}_{i.M} - \mathrm{LC}_{i.W.R} \tag{2}$$

where $LC_i$ is the measured external load, $LC_{i.M}$ is the measured total force, $LC_{i.W.R}$ is the reference load presented in Table 1 and $i$ and $S$ denote the load cell and winter, respectively.

The same approach was used for the stress cells, but here the recorded stress when the panels were submerged in the water was used as the reference stress.

$$\sigma_j = \sigma_{j.M} - \sigma_{j.R} \tag{3}$$

where $\sigma_j$ is the measured pressure, $\sigma_{j.M}$ is the unadjusted measured stress, $\sigma_{j.S.R}$ is the reference stress as presented in Table 1 and $j$ denotes the stress cell.

The three load cells installed in the load panel calibrated and validated in the laboratory before the installation of the panel. An external load was applied via a hydraulic jack. Four calibrations were performed, with the load placed either at the center of the panel and over each load cell. The external load was increased to a maximum value of 800 kN and 700 kN for the centric and eccentric loads, respectively. Based on the calibration, a correction factor of 1.25 is used to account for the part of the load that is carried by the seal; the total load of the load panel is thereby calculated as

$$\mathrm{LL}_{\mathrm{LP}} = 1.25\left(\frac{\mathrm{LC}_1 + \mathrm{LC}_2 + \mathrm{LC}_3}{w_p}\right), \tag{4}$$

where $LL$ is the line load in kN/m, and $w_p$ is the width of the load panel (1 m). The average error for the measured load for the hydrostatic pressure is 0.5 kN/m, with a standard deviation of 2.0 kN/m (Hellgren et al., 2020).

At each panel, the sensors measure the ice pressure at four depths. The measured stresses are interpolated over the thickness of the ice to a line load. In this study, three methods were used for the interpolation. In the first method, the line load is calculated as the average stress measured at each panel multiplied by the total ice thickness.

$$\mathrm{LL}_{\mathrm{SCP}.X}(t) = \frac{h_i(t)}{J_a(t)} \sum_{j=1}^{J_a(t)} \sigma_{X.j}(t) \tag{5}$$

where $LL_{SCP.X}(t)$ is the line load (kN/m) of Panel $X$ (A-D) at the time $t$, $h_i(t)$ is the ice thickness, $J_a(t)$ is the number of active stress cells. The ice thickness measured 0.3 m from the dam line was used for Panel A-C and the thickness at 6 m for panel D. The thickness was interpolated linearly for the time of the ice thickness measurements.

However, the first method may underestimates the total ice load when a large part of the load is the pressure above the top sensor. A more correct method for estimating the whole ice pressure is likely to include the associated ice thickness for each sensor. Based on the position of the ice, each sensor is assigned a representative thickness of $h_{i.j}$, and the total load is calculated as.

$$\mathrm{LL}_{\mathrm{SCP}.X}(t) = \sum_{j=1}^{J_a(t)} \big(\sigma_{X.j}(t)\big) h_{i.j}(t) \tag{6}$$

The sum of the representative ice thickness is equal to the total ice thickness. To calculate the line load with Eq. (6) require the level of the

top and bottom of the ice as input. Two assumptions were used to estimate those levels. In the first approach, the ice is assumed to follow the fluctuation of the water. The fraction of the ice submerged in the water level is equal to the ratio between the density of ice and water. Here, the density of the ice was assumed to be 918 kg/m$^3$. In the second approach, the ice is assumed to be frozen to the dam wall so that the top of the ice sheet is constantly at level +350.6, the level of the top of the ice sheet when the stress cell panels were installed.

When only one stress cell is used, Hoseth and Fransson (1999) propose that line load is calculated based on the assumption that the pressure has a linear variation between the top and bottom of the ice, with maximum stress at the ice surface and zero at the bottom,

$$\mathrm{LL}_{\mathrm{SC}}(t) = \frac{\sigma_{\mathrm{SC}}(t)}{2} \frac{h_i(t)^2}{h_i(t) - y_{\mathrm{SC}}}, \tag{7}$$

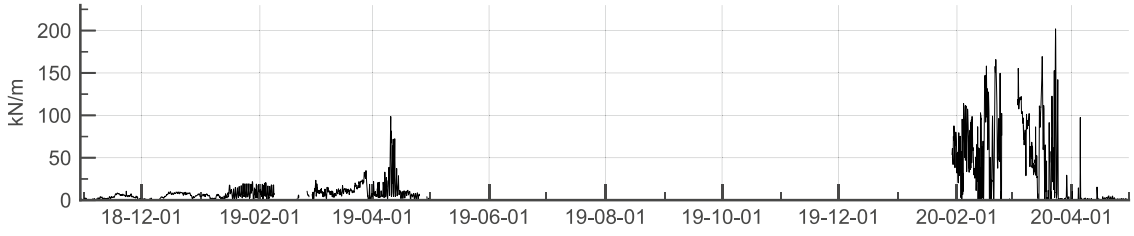


(a)

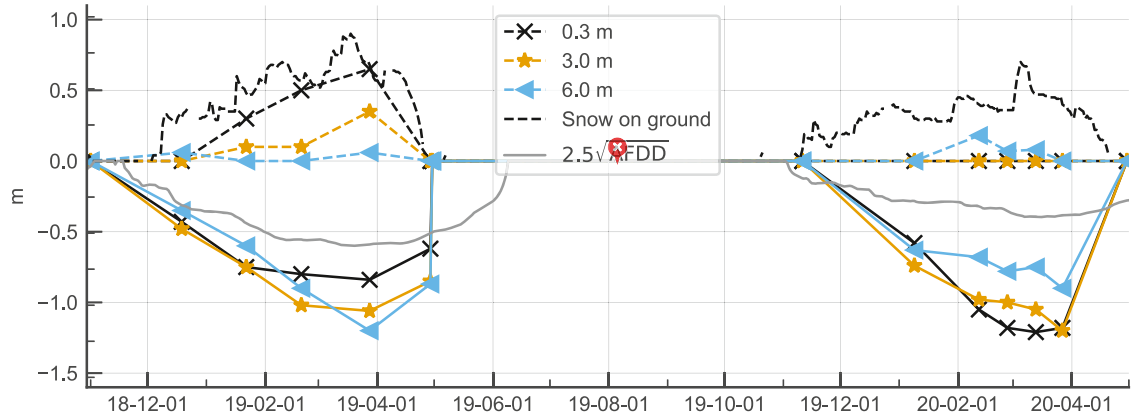


(b)

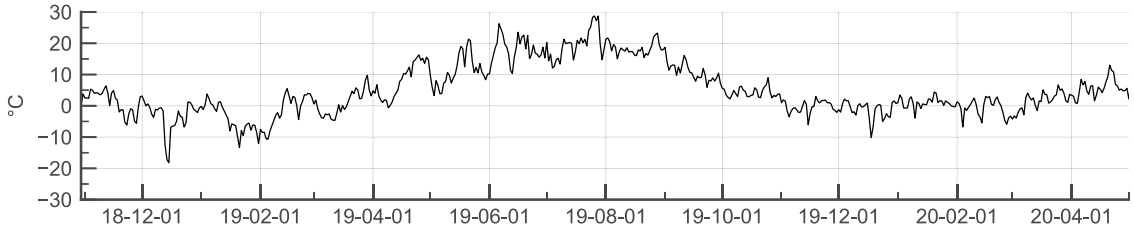


(c)

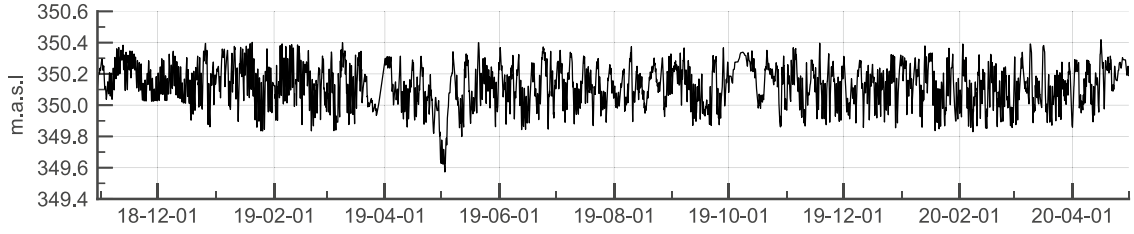


(d)

**Fig. 4.** (a) Measured ice load, (b) Measured and estimated ice thickness at 0.3 m, 3.0 m and 6.0 m from the dam, measured snow cover on the ice at the same location, snow cover on the ground and estimated ice thickness based on AFDD, (c) outside air temperature and (d) water level.

where $y_{SC}$ is the vertical distance from the middle of the sensor and the top of the ice sheet.

### 2.4. Event identification

Ice loads are often categorized into ice load events (Comfort et al., 2003). An ice load event is characterized by the rise and subsequent fall in ice load around a local peak value. An ice load event varies typically from a few hours to several days and the length of the event is mainly a function of the loading mechanism. Such events are by nature ad-hoc, as they only can be identified after the ice load is known. An alternative event-based approach is to identify events from the mechanisms that causes ice load. For dams, these mechanisms are mainly air temperature and water level changes (Carter et al., 1998; Comfort et al., 2003). Unlike ice load events, mechanism-based events have the potential to predict ice loads in places where the ice load is unknown.

In this study, ice load events, air temperature change events, and water level change events were identified. To identify such events, a search was performed to find local maximums and minimums in the recorded signals. A local maximum or minimum was defined as the extreme value during at least 12 h. This search was performed somewhat differently between the ice load and the other variables. For the ice load, a threshold value was applied to neglect local peaks with a value less than 75 kN/m. After identifying a peak in the ice load signal, an iteration was performed to find the nearest previous local minimum. This algorithm finds ice load events where the load increases.

For the other variables, no threshold was used, and in addition to finding the previous local minimum, the iteration was extended to find the most immediate following local minimum. Hence, allowing for thermal and water level events to include both increases and decreases for the temperature and water level, respectively. The search was performed with the Argrelextrema function from the Signal subpackage of the SciPy package (Virtanen et al., 2020).

## 3. Results and comments

### 3.1. Load panel and ice thickness

Fig. 4 shows the maximum daily measured ice load during the winters 2018–19 and 2019–20 together with the measured ice thickness, snow cover, snowfall, air temperature, and water level in the reservoir. Winter 2018–19 was a quiet winter in terms of ice loads. Just as in previous measurements, only small loads were measured during the early winter to early January. In mid-January, the ice load shows a daily variation correlated to the water level in the reservoir. During this winter, however, these peaks are low and do not exceed 25 kN/m. The highest ice loads this winter are measured in April. On 10 April, 11 April, and 12 April, the daily peaks in ice load was 100 kN/m, 73 kN/m, 74 kN/ms, respectively. These three values are the three highest values throughout the winter.

The time history of the ice load from the winter 2019–20 winter differs from the previous winter. No data are available before January 2020 this winter. Hence, the ice loads during the early winter are unknown. However, these are expected to be small according to the recordings from previous years. During February and March, the measured load is large and volatile. The winters' and the new all-time peak values for the load panel of 202 kN/m are measured on 23 March. This peak occurs as part of three consecutive days with high peaks. The measured ice load exceeds 150 kN/m on six occasions during this winter.

Fig. 4b shows the measured thickness together with the estimated ice thickness from Eq. (1) and the accumulated snowfall on the ground. During the first winter, the ice is the thinnest closest to the dam and thicker further out in the reservoir. The opposite relationship applies to the snow, where the snow has gathered closest to the dam. This is mainly due to snow being plowed on to the ice from the overpassing bridge but can also be an effect of snowdrift from the wind. A large proportion of the ice is reported as snow ice. More specifically, the average ratio of snow ice thickness to the total ice thickness, from the first to the last measurement occasion, are 0.73, 0.66, 0.44, 0.67, and 0.90. The second winter, the ice sheet is almost completely snow-free during the whole winter, despite the relatively large snow cover on the ground (0.7 m). One possible explanation for this is that the combination of the mild winter where the temperature varied around zero and the water level variation meant that the snow melted to water and that growth of black ice could occur from the top ice surface. In contrast to the previous winter, the ice closest to the dam this year was considerably thicker than the ice further out in the reservoir. The ice character also differed from the previous year, and no division between black ice and snow ice could be seen as the ice sheet had solid properties. For both winters, the maximum ice thickness occurred in late March and was 1.2 m and 1.18 m for the winters 2018–19 and 2019–20, respectively.

As the amount of snow on the ice is the most important factor for differences in ice growth between winters (Ashton, 2011), it is likely that the difference in ice formation between the two winters is caused by the difference in the amount of snow on the ice, especially near the dam.

Notably, the ice thickness near the dam exceeds the thickness estimated with Stefans equation with more than a factor of two. Hence, the measured ice thickness of 1.2 m from 2019–20 is not probable without either superimposed ice formation, accretion of large volumes of frazil ice at the bottom, or mechanical deformation such as rafting. Our hypothesis is that a combination of the snowfall, the mild winter, and the frequent variations in water level has caused significant surface ice growth. The water level fluctuation results in frequent flooding, and the ice can thus grow directly from the top of the ice. Our observations indicate that during winters with relatively lesser snowfall, the snow that lands on the ice is mixed with the water and then becomes part of the ice. The outdoor air temperature at the dam is presented in Fig. 4c. During both winters, the larger ice loads are measured in periods when the temperature varies around zero.

### 3.2. Variation between winters

Several factors may influence the magnitude of the ice load. These factors can be divided into variables that vary between dams and variables that vary between winters. In the former category are, for example, the reservoir shape and the stiffness of the dam (Ko et al., 1994; Comfort et al., 2000; Hellgren and Malm, 2020). This section focus on factors in the latter category, those that vary between winters. Thus, this results show relation between the ice load and variation in external factors between winters, as the reservoir and dam are constant.

Table 2 shows the maximum annual value of the ice load and selected external factors. Based on data from the five winters, the tendency is that the maximum ice load for a winter is positively correlated with the average frequency of water level change and the minimum temperature during the winter and negatively correlated with the snow on the ice, the cumulative snowfall and the AFDD. These results indicate that the largest ice loads at Rätan dam occured during relatively mild winters with little snow. This finding is not in line with previous proposals to determine the design ice load as increasing with the winter's minimum temperature or AFDD (Fransson, 1988; Ko et al., 1994; Carter et al., 1998). A note of caution is due here since the possible influence from the addition of the load panel before the last winter and the limited amount of data. Further, the variable that affects the difference between winters in ice load magnitude may differs between dams and may be different than those causing a difference in ice load between dams. In future studies, data from previous measurements from the literature should be included in such an analysis.

### 3.3. Ice load events

In Fig. 5, all identified ice load events larger than 75 kN/m are presented. In the figure, the associated variation in temperature and

**Table 2**
The recorded maximum annual recorded ice load, number of ice load events and selected external factors. The presented external characteristics of the five-winters are average amplitude and average frequency of water level change; maximum ice thickness at the dam wall; maximum measured snow cover on the ice at the dam wall and cumulative snowfall in water equivalent; the minimum daily mean temperature and maximum daily temperature difference; and AFDD.

| Winter | Ice load | | Water level | | Ice thick. | Snow | | Temperature | | AFDD |
|---|---|---|---|---|---|---|---|---|---|---|
| | Max kN/m | Events N | Avg. Amp m | Avg. Freq N/day | Max m | Max m | Cum WE mm | Min °C | Max diff °C | Max °C days |
| 2015–16* | 160 | 7 | 0.22 | 1.31 | 0.80‡ | – | 200 | −21.4 | 12.0 | 646 |
| 2016–17* | 168 | 24 | 0.20 | 1.16 | – | – | 276 | −17.3 | 19.6 | 405 |
| 2017–18*† | 59 | 0 | 0.28 | 1.01 | – | – | 334 | −19.0 | 13.3 | 898 |
| 2018–19 | 99 | 1 | 0.24 | 1.12 | 0.84 | 0.65 | 287 | −19.4 | 12.1 | 576 |
| 2019–20§ | 202 | 41 | 0.24 | 1.29 | 1.21 | 0.00 | 273 | −11.6 | 8.92 | 251 |

* From Hellgren et al. (2020).
† No recordings from March and April.
‡ From one measurement, taken in February
§ Dummy panels added to the measurement design.

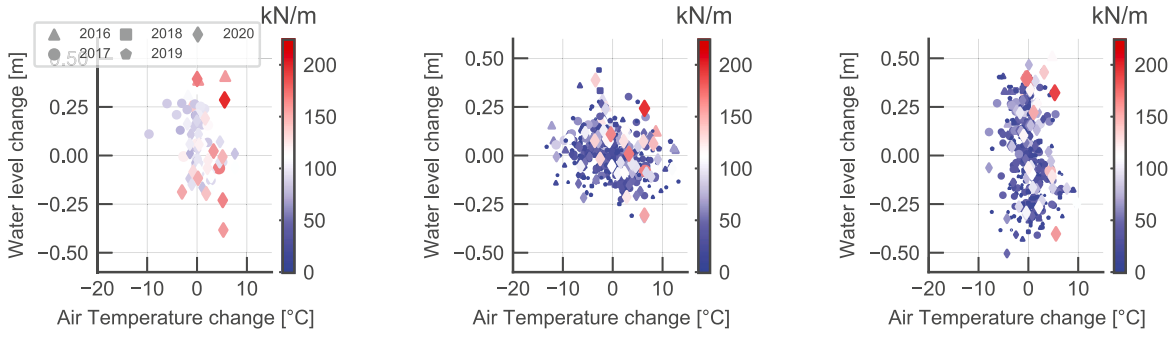


**(a)** Ice load than greater than 75 kN/m

**(b)** Thermal events during Jan, Feb, and March

**(c)** Water level events during Jan, Feb, and March

**Fig. 5.** Event peak ice load as a function of the change in air temperature and water level from the start to the end of the event. (For interpretation of the references to color in the text, the reader is referred to the web version of this article.)

water level from the start to the end of each ice load event is presented on the *x*- and *y*-axis, respectively. The magnitude of the ice load is shown with the color and size of the marker, while the marker type denotes the winter. Overall, the results show significant scatter where large ice loads are present in three of four quadrants, and these may occur after both an increase or decrease in the external variables. Comfort et al. (2003) found that a combination of water level change and positive temperature change produces the largest ice loads. Similar results where found in this study where a simultaneous decrease of the temperature and increase of the water level is the only combination of events that are not associated with ice loads greater than 100 kN/m. The overall maximum measured load of 200 kN/m from 2020 is associated with a relatively large increase in both the temperature and the water level. In 2020, several of the significant ice loads are occurring after a relatively large lowering of the water level. This pattern differs from previous years when an increase in water level was associated with significant ice loads.

Fig. 5a and c show the identified events of variations in temperature and water level respectively and the associated peak ice load during such an event. The figure shows events from January, February, and March during the five measurement winters. One unexpected finding was significant ice load when there is no water level change and no or even a negative temperature change. These ice loads may be caused by the third ice load generating mechanism, shear forces from wind and water currents (Carter et al., 1998; Comfort et al., 2003). However, the water currents should be strongly correlated with changes in the water level. Another explanation for these results may be flooding of the ice from cracks formed during thermal contraction. At previous measurements at Taraldsvikfossen (Petrich et al., 2015), flooding was observed during cold spells. This flooding caused the ice temperatures to increase rapidly, resulting in a thermal load.

In addition, the surprising results are partly explained by the use of local minimums in the ice load signal as the start time for an event. This choice means that some events identified from the ice load signal include an initial period following the minimum with a relatively slow load increase. This initial period ends near a min or max in the external variable and is followed by a larger increase in ice load when the external variable change in the opposite direction. Hence, for some events, the difference in temperature from the start and the peak is negative, although the majority of the ice load increases occur during a temperature increase. In future investigations, it might be possible to improve the identification of ice load events by using a rate-dependent definition.

In contrast, the results in both figures show that combinations with the largest absolute distance from the origin often result in small ice load events with peak ice loads smaller than 50 kN/m. Similar results were found by Petrich et al. (2015), where not all thermal change events resulted in stress peaks.

The results shown in the figures suggest that a major change in temperature or water level, or any combination of these, is alone not sufficient to create an ice load event. A possible explanation for this might be that thermal ice loads appear when the air temperature change causes an ice temperature change, and the dam restrains the resulting thermal expansion of the ice. The restrained displacement of the ice also causes ice load from water level variation. Therefore, in addition to a water level or temperature change, additional conditions must be satisfied to create this restrained force. Future research should aim to quantify the additional prerequisites required to create an ice load event. Examples of such mechanisms are the re-freezing of cracks in the

ice (Comfort et al., 2003).

### 3.4. The influence of the dummy panels

Fig. 6 shows a box plot of the distribution of the measured ice load with the load panel during the spring (Jan-April) of the five winters. Included in the figure are months where the sampling was active for more than ten days. The results in this figure, Figs. 4, 5, and Table 2, indicate that the measured loads from February and March in the spring of 2020 differs from the previous years. For all of the maximum load, the variance and the median load, the two largest values, so far, were recorded during these two months. However, the most significant difference is the more considerable variation in pressure with a more substantial proportion of high values and the large number of ice load events. As shown in the previous paragraph, the 2019–20 winter was relatively mild and snow-free, but the ice thickness near the dam was 0.4 m thicker in 2020 than in 2019. These factors may have caused the difference in the load exerted on the panel. The other possibility is that new dummy panels have decreased the panels' influence on the naturally formed ice sheet and that the behavior measured this winter is a more accurate measurement of the true shape and magnitude of the load on the dam from the ice.

Fig. 7 shows photographs of the crack in the ice along the dam from 2017 and 2020. From the previous winters, there was a clear disturbance of the naturally formed crack around the load panel, as can be seen in Fig. 7a. The crack in the ice had a curved shape around the panel, and there was a collection of snow and ice in the direct proximity of the panel. It is hence obvious that ice near the panel differed from the other ice along the dam and that the panel was disturbing the ice. After the installation of the dummy panels, this disturbance around the load panel is not present anymore, as can bee seen in Fig 7b. There is accumulation of snow ice along the dummy panels and load panel, but similar accumulation is present along the rest of the dam, and there is only a minor difference between the dam line and the panel.

Based on the measurement and observation, this study conclude that the earlier design of the load panel affected the ice sheet and possibly the measurement result. However, with only one winter with the dummy panels, it is too early to draw any definite conclusions. However, for any future measurements with a load panel, our recommendation is to use several panels and a dummy panel to increase the length of the undisturbed surface around the sensors.

### 3.5. Stress cells

#### 3.5.1. Broken cells and anchorage of the frames

At the end of the ice, only two stress cells were still functional (CPA4 and CPB2). The signal from the stress cell sensors was gradually lost during the latter part of March, with a peak of six sensors lost sensors during the night between 29 March and 30 March. For the nonfunctional stress cells, cable failure had occurred for three sensors, and a total loss of function had happened for the remaining seven. In addition to the damaged stress cells, the steel frames were also strongly affected by the ice. Fig. 9 shows photographs of frames A and B, taken in early April when the stress cell in the ice was removed. All three frames have been subjected to a downward vertical tensile force large enough to cause severe plastic deformations of the frames. The frames were damaged sometime between 2020-03-13 and 2020-03-27. After the damage or the failure of one of the stress cells at a frame, the adjacent sensors' accuracy cannot be guaranteed. Therefore, only data from before the first sensor on each frame stopped function is included in summaries and analysis. However, for transparency, all recorded data are presented in the next section.

That both the stress cells and the frames were broken shows that the local conditions at the dam-ice contact are harsh. Compared to the load panel with a massive steel lid, the stress sensors are thin and less robust. For a setting like this, with ice thickness over 1 m and small but daily water level variations, installing such sensors in a frame directly on the dam face may be inappropriate. During earlier measurements in Taraldsvik (Petrich et al., 2020), similar frames and the same cells were used. The frames were attached to the bridge on the dam with timber studs. That attachment failed during the ice break, but the stress cells and frames remained intact. In this project, the timber studs were replaced with plates of steel to ensure that the cells and frames were firmly anchored to the dam. Hence, it is possible that the steel attachment is too stiff and that the robust anchoring caused the cells and frames to fail.

To further use stress cells in reservoirs with frequent water level variation, a recommendation is to install the cells at a small distance from the dam in the ice and allowing the sensors to move with the ice sheet. If the cells are installed on the dam face, one approach not tested is to grout them to the dam wall. Alternatively, the anchorage should be designed to fail before the frames to allow for some vertical movements to protect the sensors. This does, however, influence the expected accuracy of the sensors after such anchorage failure.

The sensor in the ice was removed on 2 April. At this time, the total

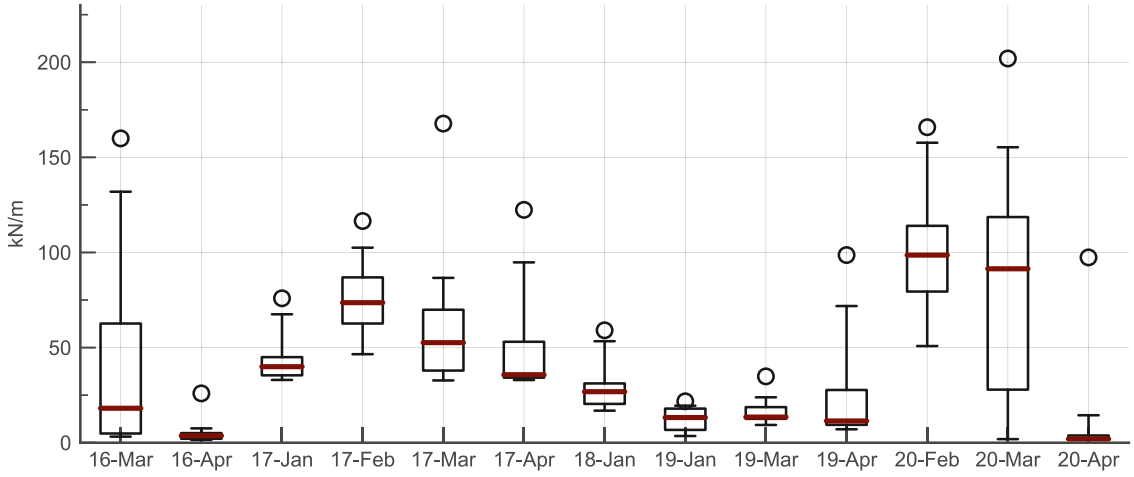


**Fig. 6.** Box plot of the distribution of the measured ice load with the load panel during the spring of the five winters. Included in the figure are all months where the sampling was active for more than ten days. Each box shows the median (red) value; the bars extend from the lower to upper quartile values, and the whiskers include 95% of the measured values. The maximum measured load for that month is marked with a circle. (For interpretation of the references to color in this figure legend, the reader is referred to the web version of this article.)

(a) (b)

**Fig. 7.** Photographs of the crack in the ice along the dam line from (a) 2018, and (b) 2020.

ice thickness near the sensor was 1.1 m and 1.08 m, with no snow on the ice and more than 0.2 m of black ice had formed over the sensor since it was installed in January. The sensor was located in a small pocket of water in what was otherwise solid ice. This indicates that the stress cell heats the ice locally, causing the ice to melt. This heating is probably caused by solar absorption by the stress cell. The impact of the melted ice around the sensor is difficult to quantify as the timing of the phase changes near the sensor are unknown.

#### 3.5.2. Recordings

Fig. 8 shows the temperatures and stresses in the ice measured by the stress cells. The figure is distributed in the four sensor levels. For example, all top sensors' measured stress and temperature are shown in the top and second top subfigures. Except for Panel A, only the upper layer of sensors has measured a significant temperature variation. This is expected for the lower level sensors as the temperature in the interface between ice and water is 0 °C. These results indicate that the cold outside air temperature only penetrates the top layer of the ice. The exception to this is For Panel A, where temperatures as low as −7 °C are measured at the bottom positioned sensor. For this panel, high stresses have been measured at the lower level while the rest of the level four sensors recorded stresses near zero during the whole measurement period.

The sensor placed in the ice shows large variations in temperature during February. This variation in temperature is visually correlated with the measured stresses. Tests for time-lagged cross-correlation show that local peaks of correlation occur for 2, 27, 48, and 72 h phase-lag between the stress and temperature. The peak correlation of 0.21 is for a 48-h lag. However, the stress temperature relation is not expected to be linear. In both the temperature and stresses, a combination of a long cold period and daily variations between night and day can be seen. In March, the temperature variation at the location of the sensor stops, and except for two shorter periods, the temperature remains constant at 0 °C. During both of these temperature drops, the temperature differences give rise to subsequent stress variation. On the first occasion in mid-March, these measured stresses are relatively small in relation to the temperature variation. On the second occasion, the temperature variation is smaller but causes a more significant stress peak. The first peak in measured ice pressure after an extended period with temperatures at or above zero degrees is an artificial freeze in pressure that can be as large as 1 MPa (Hoseth and Fransson, 1999; Carter et al., 1998). It is likely that the second peak is such an artificial local pressure and that the measured stresses are not representative of the global stresses in the ice sheet. Overall, the stress measured by sensor CPD1, placed in the ice, strongly correlates with the temperature.

For the panels mounted on the dam, the relation between temperature variation and stress variation is almost non-existing. This is particularly evident for the second and third layers of sensors, where the temperature variation is virtually non-existent, while stresses above 1 MPa are recorded by all cells.

### 3.6. Comparison of load panel and stress cells

Fig. 10 show the measured total line load calculated with Eqs. (4) and (5) from spring 2020. In the line load calculations for the stress cell readings above 1000 kPa, the measurement range of the cells was removed. For panels A–C, the ice load is calculated using the three different interpolation methods. In general, all methods give equivalent results. However, on several occasions, the difference between calculated line loads exceeds 100%. This additional uncertainty occurs when the water level fluctuates, and the ice's position relative to the sensors is not obvious. It can also be seen that the volatility in the ice load increases when the number of active sensors decreases. When the loads are calculated from only one sensor, it is an extrapolation based on stresses measured from less than 10% of the ice's cross-section. The results in Fig. 10 show that the daily variation becomes unreasonably high when such extrapolation is used.

Table 3 presents the maximum interpolated load from the winter. For the stress cell panels, the table presents the maximum from the period before the failure of the first stress cell at each frame, respectively. Overall, the total interpolated load measured by the stress cells is great and, unrelated to interpolation method, the recordings by the three

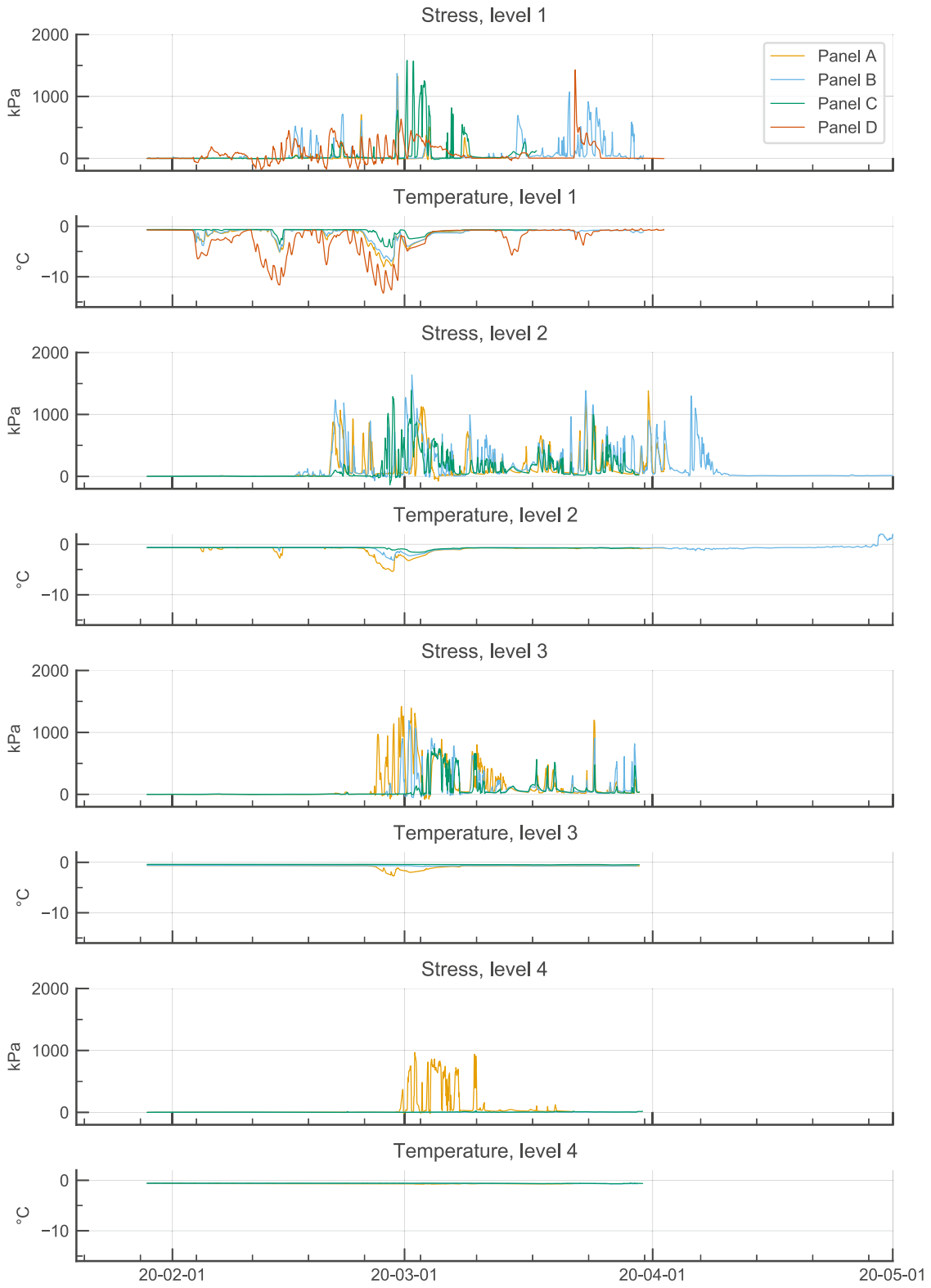


**Fig. 8.** Measured stresses and temperatures with the stress cells. Each pair of stress and temperature plot shows the results from on layer of sensors, i.e., all stress cells with the same relative position.

stress cell panels at the dam are among the historically largest measured ice loads. The previous maximum load of 780 kN/m was recorded by Bisanswa (2011), who used a similar sensor configuration at two dams. The result from this study and Bisanswa (2011) are similar, both with regards to the time history and season maximum load. Other historic top recordings of interpolated loads from stress cells panels at the dam walls are: 600 kN/m from one winter with four panels at La Gabelle (Bisanswa, 2011); 270 kN/m from from five winters with three to four panels at Tradalsvik (Petrich et al., 2020); and 200 kN/m from one winter with eleven panels at Barrett Chute dam (Côté et al., 2012). For comparison, historic top recordings with biaxial gauges are; 370 kN/m from five winters at Seven sisters dam (Comfort et al., 2003), 290 kN/m

**(a)** Frame to Panel A **(b)** Frame to Panel B

**Fig. 9.** Photographs of the frames from 2020-04-02.

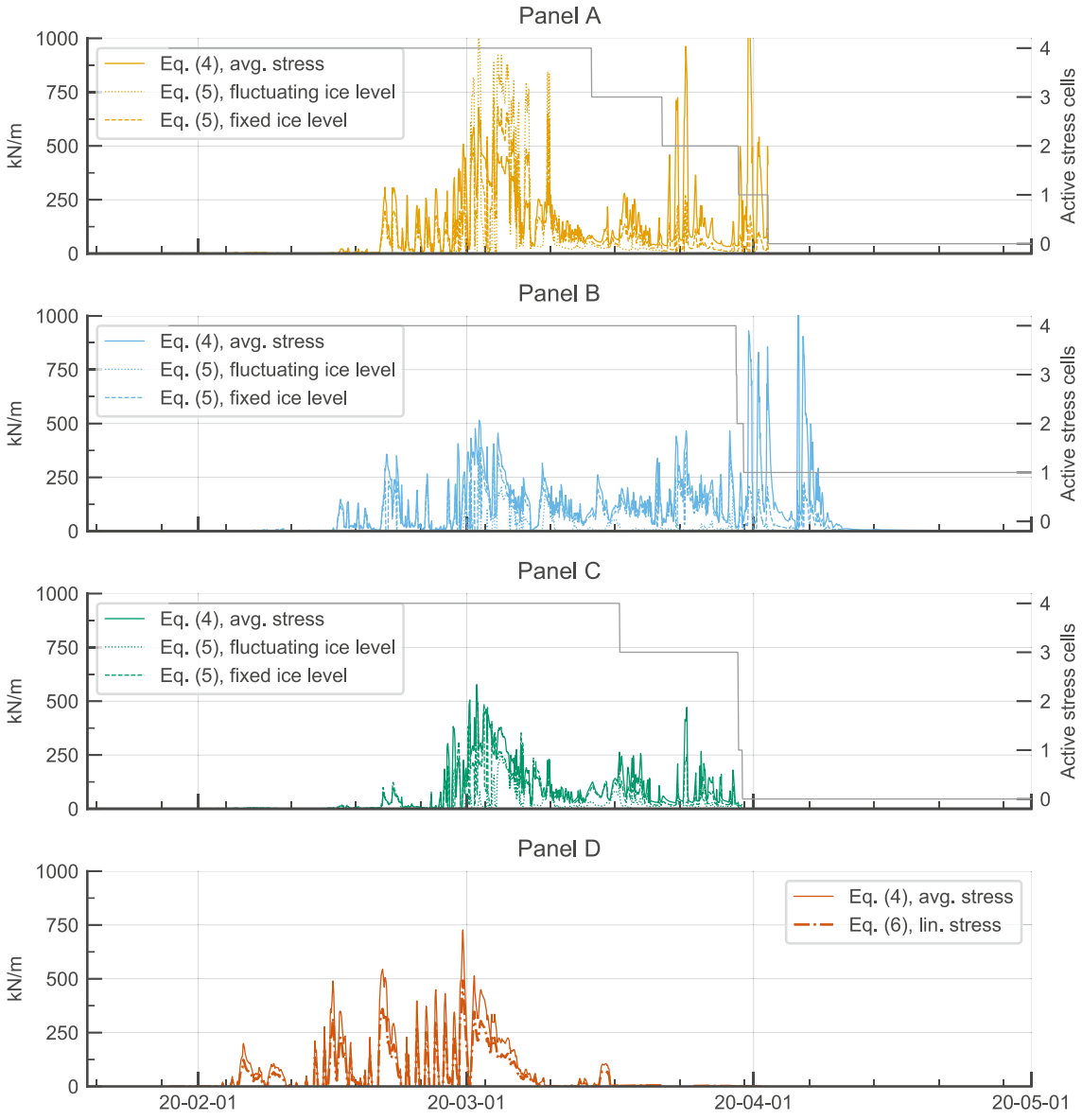


**Fig. 10.** The measured line load from the four panels attached on the dam and the average load from those panels weighted by sensor width.

**Table 3**
The ice load's maximum value for the four stress cell panels calculated with the four methods and the sensor width weighted average.

| | Eq (4) kN/m | Eq. (5), fluct. IL kN/m | Eq. (5) fixed IL kN/m | Eq. (6) kN/m |
|---|---|---|---|---|
| Panel A | 680 | 1000 | 720 | – |
| Panel B | 520 | 210 | 390 | – |
| Panel C | 580 | 270 | 490 | – |
| Panel D | 730 | – | – | 490 |
| WAVG A, B, C, LP | 480 | 400 | 410 | – |

from four winters at Eleven Mile Canyon dam (Monfore, 1954).

Fig. 11 shows a matrix plot of the maximum daily measured ice load with the four panels for the period 14 February to 2 April. The matrix plot shows the relation for parings of the sensors. The diagonal of the matrix shows a bar plot for the recordings from each panel. The lower left and the upper right part shows an array of scatterplots and Pearson's correlation for each possible combination of panels, respectively. For the stress cell panels, data after the failure of the first stress cell at the respective frame is excluded from the analysis. The period was chosen to start three weeks after the installation of the stress cell and to end when the stress cell in the ice was removed. The correlation between Panel A, B, and C is between 0.75 and 0.86, a range commonly used to indicate a high degree of correlation. The three stress cell panel, thus, appears to measure the same physical process. However, the correlation between the stress cells and the load panel is low. All panels are exposed to the same external conditions in terms of snow, temperature, and water level change. Therefore, it is surprising with such a low correlation.

There are several plausible explanations for the difference in recorded results:

1. The set-up used for the stress cell are not suitable for this type of condition.
2. The ice load varies considerably along the dam.
3. Difference in sensor technique.
4 Difference in the time of installation, i.e., before or after ice formation.
5 Inadequate handling of the sensors.

Each of the above explanations has different implications for the conclusions of this study. The first explanation, the suitability of the sensors for this type of condition are discussed above in the section about the damaged frames and broken sensors.

The second explanation, that the ice load varies considerably along the dam, even over shorter distances, is in line with previous studies. Taras et al. (2011) showed that the stress in the ice and the resulting load acting on the dam can have a significant spatial variation and can vary significantly over a distance of a few meters along the dam simultaneously. Simulations by Hellgren and Malm (2020) show, from a thermal elastic perspective, such variation is expected, and that variation in

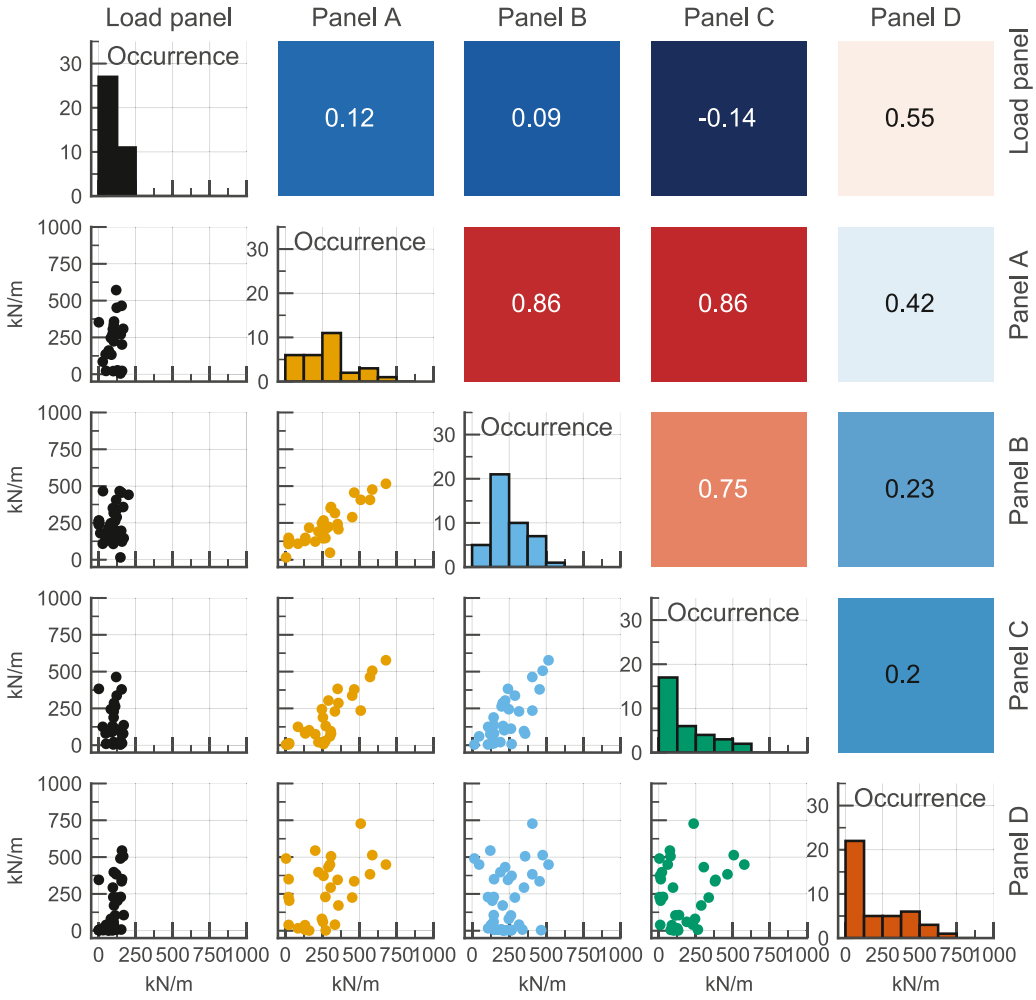


**Fig. 11.** Matrix plot of the correlation between the measured maximum daily load by the five panels. The upper part shows a color map of the Pearson correlation. The scale is from blue (0) to white (0.5) and red (1). The diagonal shows histograms of the loads from each panel. The lower part shows a plot of the measured load as a function of the other sensors. (For interpretation of the references to color in this figure legend, the reader is referred to the web version of this article.)

ice pressure along an individual monolith can be significant. The variation along the dam, within individual monoliths, is in the simulations over 400% and more than 100 kN/m between monoliths. Such behavior would cause the measured ice load to be greater for the load panel and Panel B, positioned over the stiffer part of the monolith. Instead, there is a tendency for the ice load to be greatest at Panel A and C.

This conclusion would devalue several of the previous ice load measurements, including the load panel results, which have occurred at only one or a few locations on the dam. Furthermore, in the literature, the static ice load on dams is often modeled as a function of the external conditions using a 1D or 2D model that does not consider the spatial variation along the dam (Comfort et al., 2003; Kharik et al., 2018; Petrich and Arntsen, 2018; Hellgren et al., 2019). Assume that a model is created which correctly predicts the ice load at one point along the dam during a winter. The same model could over-or underestimate the ice load only 3 m from the first, with 200%. The external factors do not differ significantly over 3 m, which means that other factors such as the formation of cracks in the ice and randomness in the wind, water, and snow, may affect the ice load.

An alternative way to solve this issue could be to measure ice stresses in the reservoir. Such a solution is not as representative for the ice load acting on the dam and involves its own disadvantages. However, this placement may provide a reasonable estimate of the average ice load. Côté et al. (2016) showed that the mean value from eleven panels placed separated along the dam wall with a distance of 2.5 m corresponded well with the measured ice load from one of their three panels placed in the ice. Based on this, Côté et al. (2016) derived a hypothesis that the loads measured by sensors locally at the wall register noise caused by the dam-ice interaction. This noise is then averaged further out into the reservoir, and ice load at a distance x from the dam is equal to the average load over a distance equal to 2×. In this study, only one stress cell was used on Panel D, placed in the ice. Hence, any comparison between the results from Panel D and the other panels is subject to significant uncertainty. However, the correlation between Panel D and the load at the dam is low for all stress cell panels and moderate for the load panel. The moderate correlation between the load panel is an indication that the relationship between stresses at the dam and in the ice is worth further investigation. An alternative interpretation to the results from Côté et al. (2016) is that the added sensor area from averaging the eleven stress cell panels makes the total area more representative of a dam monolith. In this case, the load panel's recording and the combination of the load panel and stress panels from 2020 are a good approximation of the average ice load. The load panel alone has a greater ice contact area the ice contact area of the elven stress cell panels combined. All this considered, it is essential to focus further studies on the ice load's spatial variation over an entire dam and establish how the average pressure decreases over a complete dam and with added sensor area compared to local stresses.

This study compares stress cell measurements in the ice with load panel measurements at the dam wall. Previous studies have often used both stress cells and biaxial gauges for ice stress measurements and found agreement between the two techniques (Taras et al., 2011; Morse et al., 2011; Côté et al., 2012; Comfort et al., 2003). The discrepancy in measured load in this study indicates a need for further studies that quantify the choice of sensor influence on the observed loads.

## 4. Conclusions

This paper presents ice load measurements with several sensor types from a concrete dam during winters 2018–19 and 2019–20. A $1 \times 3\ m^2$ load panel attached to the dam face measured the ice pressure during both winters. The measurement's design was updated before the winter 2019–20 whit the installation of two $2.75 \times 1.75\ m^2$ dummy panels adjacent to the load panel. During spring 2020, the ice pressure was measured with an additional 13 pressure cells. Four stress cells were placed on a steel frame to form a load panel. The three panels were placed on the upstream face of the dummy panels. One single stress cell was placed 6 m out in the reservoir in front of the load panel.

The panel measured seasonal maximum ice load 100 and 200 kN/m for the two winters, respectively. Winter 2019–20, when the panel measured the largest loads, was mild for the location, with great ice thickness near the dam face (1.18 m), an almost snow-free ice sheet throughout the winter, and frequent water level variations (1.3 per day). Installing the dummy panels reduced the load panel's impact on the ice sheet near the panel significantly, as evident by the crack-pattern of the ice sheet near the load panel. The time history of the measured loads after installing the dummy panels differs from the loads measured before. It is still too early to determine if the difference is caused by the dummy panels or the differences in the external conditions between winters.

The load panel recorded large ice loads (>75 kN/m) for all combinations with increasing/decreasing air temperature and/or water level. Identification of temperature change events and water level change events during the winters, shows that a change in temperature, water level, or any combination of these, is not sufficient alone to produce large ice loads at Rätan. These findings suggest that other conditions must be satisfied before a water level or temperature change results in large ice loads.

The majority of the stress cells recorded ice pressure larger than their measurement range. At the end of the ice season, only two of the panels' twelve stress cells were still functional, and the ice vastly deformed the steel frames. Extra measures to protect the sensors must be taken when installing the stress cells directly on the concrete face in conditions with ice thickness over 1 m and small but daily water level variations. Different assumptions for the interpolation used when calculating the line load from the stress cells may alter the resulting line load significantly. From the period before the frames were damaged and unrelated to the interpolation method, the recordings by the three stress cell panels at the dam are among the historically largest inferred ice loads.

## Data availability

The data and code that support the findings of this study are openly available in Mendeley data at https://doi.org/10.17632/gsrrtr28hp.1. From the data and code, all figures and tables presented in this paper are fully reproducible.

## Funding

"Swedish Hydropower Centre – SVC".

## Declaration of Competing Interest

Rikard Hellgren was also employed by WSP Sverige AB and Richard Malm by SWECO Energuide AB. At WSP and SWECO, Hellgren and Malm acted as dam safety consultant primarily hired by the Swedish energy companies. Christian Petrich and Bård Arntsen are board members of Ice Mate AS, a company that develop, produce and sale technology and solutions for monitoring and reduction of ice loads on dams.

## Acknowledgments

The research presented was carried out as a part of "Swedish Hydropower Centre – SVC". SVC has been established by the Swedish Energy Agency, Elforsk, and Svenska Kraftnät together with Luleå University of Technology, KTH Royal Institute of Technology, Chalmers University of Technology and Uppsala University. www.svc.nu. CP and BA wish to acknowledge support from the Research Council of Norway FORREGION program, grant number 280744 (BA Senter Nord) and NORDSATSING program, grant number 195153 (ColdTech).

## References


Ashton, G.D., 2011. River and lake ice thickening, thinning, and snow ice formation. Cold Reg. Sci. Technol. 68 (1–2), 3–19.

Bisanswa, D., 2011. Poussée de glaces en 2009 sur les barrages de la rivière St-Maurice. Université Laval, Université Laval. Master Thesis.

Bjerkås, M., 2007. Review of measured full scale ice loads to fixed structures. In: Proc. of the 26th International Conference on Offshore Mechanics and Arctic Engineering, Number 1. San Diego, USA, pp. 1–10.

Carter, D., Sodhi, D., Stander, E., Caron, O., Quach, T., 1998. Ice thrust in reservoirs. J. Cold Reg. Eng. 12 (4), 169–183.

Comfort, G., Gong, Y., Singh, S., 2000. The factors controlling static ice loads on dams. In: Proceedings of the 15th International Symposium on Ice. Gdansk, Poland, pp. 189–198.

Comfort, G., Gong, Y., Singh, S., Abdelnour, R., 2003. Static ice loads on dams. Can. J. Civil Eng. 30 (1), 42–68.

Côté, A., Taras, A., Comfort, G., Morse, B., 2012. Hydro Quebec ice load measurement program. In: 2012 CDA Annual Conference on Dam Safety. Canadian Dam Association, Saskatoon, Canada, pp. 1–12.

Côté, A., Taras1, A., Comfort, G., Morse, B., 2016. Static ice loads at dam face and at far field. In: 23rd IAHR International Symposium on Ice. MI, USA, pp. 1–8.

Cox, G.F., Johnson, J.B., 1983. Stress Measurements in Ice. Report No. U.S. Army Cold Regions Research and Engineering Laboratory, Hanover, New Hampshire.

Fransson, L., 1988. Thermal Ice Pressure on Structures in Ice Covers. LuleåUniversity of Technology. Doctoral Thesis, LuleåUniversity of Technology, urn:nbn:se:ltu:diva-17625.

Fransson, L., 2001. Development of Ice Load Panels and Installation at Lighthouse Norströmsgrund. Report No. Low Level Ice Forces on Coastal Structures (LOLEIF) EU MAST III Project – Contract No MAS3-CT 97-0098, Hamburg Germany.

Google, 2019. Google Maps.

Hellgren, R., 2019. Condition Assessment of Concrete Dams in Cold Climate. KTH Concrete Structures. Licentiate Thesis, KTH, Concrete Structures.

Hellgren, R., Malm, R., 2020. A parametric numerical study of factors influencing the thermal ice pressure along a dam. In: 25 IAHR International Symposium on Ice. Trondheim, Norway, pp. 823–832.

Hellgren, R., Malm, R., Eriksson, D., 2019. Modelling of the Ice Load on a Swedish Concrete Dam Using Semi-Empirical Models Based on Canadian Ice Load Measurements. Sustainable and Safe Dams Around the World, vol. 2. International Commission on Large Dams, Ottawa, Canada, pp. 3068–3080.

Hellgren, R., Malm, R., Fransson, L., Johansson, F., Nordström, E., Wilde, M.W., Westberg Wilde, M., 2020. Measurement of ice pressure on a concrete dam with a prototype ice load panel. Cold Reg. Sci. Technol. 170, 102923.

Hellgren, R., Malm, R., Persson, A., Klasson Svensson, E., 2017. Estimating the effect of ice load on a concrete dams displacement with regression models. In: Proceedings ICOLD 2017 International Symposium: Knowledge Based Dam Engineering, KTH, Concrete Structures. International Commission on Large Dams.

Hoseth, K.A., Fransson, L., 1999. Istrykk pådammer Måleprogram dam Silvann. Report No. Norges vassdrags – og energidirektorat, Oslo Norway.

Kharik, E., Morse, B., Roubtsova, V., Fafard, M., Côté, A., Comfort, G., 2018. Numerical studies for a better understanding of static ice loads on dams. Can. J. Civil Eng. 45 (1), 18–29.

Ko, P.K.K., Ho, M.S.S., Smith, F., Smith, G.F., 1994. Thermal ice forces on concrete dams: recent developments. Dam Saf. 17–33.

Monfore, G.E., 1954. Ice pressure: experimental investigations by the bureau of reclamation. Trans. Am. Soc. Civil Eng. 119 (1), 26–38.

Morse, B., Stander, E., Coté, A., Taras, A., Santerre, R., Prat, Y., 2011. Spatial-temporal variability of static ice forces. In: Proceedings of the 21st International Conference on Port and Ocean Engineering Under Arctic Conditions, vol. 1. Montréal, Canada, pp. 500–509.

Petrich, C., Arntsen, B., 2018. An overview of trends and regional distribution of thermal ice loads on dams in Norway. In: Twenty-Sixth International Congress on Large Dams. International Commission on Large Dams, Vienna, Austria, pp. 1210–1224.

Petrich, C., Sæther, I., Fransson, L., Sand, B., Arntsen, B., 2015. Time-dependent spatial distribution of thermal stresses in the ice cover of a small reservoir. Cold Reg. Sci. Technol. 120, 35–44.

Petrich, C., Sæther, I., Sadnick, M.O., Arntsen, B., 2020. Static ice loads on a dam in a small Norwegian reservoir. In: 25 IAHR International Symposium on Ice. Trondheim, Norway, pp. 23–25.

Schwarz, J., Jochmann, P., 2001. Ice force measurements within the LOLEIF-project. In: Proceedings of the 16th International Conference on Port and Ocean Engineering Under Arctic Conditions (POAC'01). Ottawa, Canada, pp. 669–682.

SMHI, 2018. Swedish Meteorological and Hydrological Institute Open data opendata-download.smhi.se.

Taras, A., Côté, A., Comfort, G., Thériault, L., Morse, B., 2011. Measurements of Ice Thrust at Arnprior and Barrett Chute Dams. In: 16th Workshop on the Hydraulics of Ice Covered Rivers. Winnipeg, Canada, pp. 317–328.

Virtanen, P., Gommers, R., Oliphant, T.E., Haberland, M., Reddy, T., Cournapeau, D., Burovski, E., Peterson, P., Weckesser, W., Bright, J., van der Walt, S.J., Brett, M., Wilson, J., Millman, K.J., Mayorov, N., Nelson, A.R.J., Jones, E., Kern, R., Larson, E., Carey, C.J., Polat, I., Feng, Y., Moore, E.W., VanderPlas, J., Laxalde, D., Perktold, J., Cimrman, R., Henriksen, I., Quintero, E.A., Harris, C.R., Archibald, A.M., Ribeiro, A. H., Pedregosa, F., van Mulbregt, P., 2020. SciPy 1.0: fundamental algorithms for scientific computing in python. Nat. Methods 17, 261–272.

Zhang, M., Qiu, B., Kalhori, H., Qu, X., 2019. Hybrid reconstruction method for indirect monitoring of an ice load of a steel gate in a cold region. Cold Reg. Sci. Technol. 162, 19–34. June 2018.

Zhang, Y., Karr, D.G., Ph, D., Asce, M., 2017. Determining ice pressure distribution on a stiffened panel using orthotropic plate inverse theory. J. Struct. Eng. 143 (5).